PCCP

Nanostructure of mixtures of protic ionic liquids and lithium salts: effect of alkyl chain length

Journal:	*Physical Chemistry Chemical Physics*
Manuscript ID:	CP-ART-10-2014-004668.R1
Article Type:	Paper
Date Submitted by the Author:	12-Dec-2014

Complete List of Authors:	Mendez-Morales, Trinidad; University of Santiago de Compostela, Condensed Matter Physics Carrete, Jesus; CEA - French Atomic Energy Commission, DRT/LITEN/DTNM/LCRE; University of Santiago de Compostela, Condensed Matter Physics Rodr&#65533;guez, Julio; University of Santiago de Compostela, F&#65533;sica de la Materia Condensada Cabeza, Oscar; Universidade da Coruña, Física Javier Gallego, Luis; Universidad de Santiago de Compostela, Condensed Matter Physics Russina, Olga; University of Rome "Sapienza", Chemistry Varela, Luis Miguel; University of Santiago de Compostela, Condensed Matter Physics

Physical Chemistry Chemical Physics
CREATED USING THE RSC LaTeX PCCP ARTICLE TEMPLATE – SEE www.rsc.org/electronicfiles FOR DETAILS
ARTICLE TYPE www. rsc.org/xxxxxx | XXXXXXXX

Nanostructure of mixtures of protic ionic liquids and lithium salts: effect of alkyl chain length

Trinidad Méndez-Morales,[a] Jesús Carrete,[a,b] Julio R. Rodríguez,[a] Óscar Cabeza,[c] Luis J. Gallego,[a] Olga Russina*[d] and Luis M. Varela*[a]

Received Xth XXXXXXXXXX 20XX, Accepted Xth XXXXXXXXX 20XX
First published on the web Xth XXXXXXXXXX 200X
DOI: 10.1039/b000000x

The bulk structure of mixtures of two protic ionic liquids, propylammonium nitrate and butylammonium nitrate, with a salt with a common anion, is analyzed at room temperature by means of small angle X-ray scattering and classical molecular dynamics simulations. The study of several structural properties, such as density, radial distribution functions, spatial distribution functions, hydrogen bonds, coordination numbers and velocity autocorrelation functions, demonstrates that increasing the alkyl chain length of the alkylammonium cation results in more segregated, better defined polar and apolar domains, the latter having a larger size. This increase, associated to the erosion of the H-bond network in the ionic liquid polar regions as salt is added, is confirmed by means of small angle X-ray scattering measurements, which show a clear linear increase of the characteristic spatial sizes of the studied protic ionic liquids with salt concentration, similar to the one previously reported for ethylammonium nitrate (J. Phys. Chem. B 2014, 118, 761-770). In addition, bigger ionic liquid cations lead to a lower degree of hydrogen bonding and to more sparsely packed three-dimensional structures, which are more easily perturbed by the addition of lithium salts.

1 Introduction

Ionic liquids (ILs) are salts composed exclusively of cations and anions that are poorly coordinated, which leads to their being in a liquid state below 100 °C and even at room temperature. Due to their unique array of physicochemical properties (high thermal stability, high ionic conductivity, negligible vapor pressure, large electrochemical window and ability to solvate a wide range of organic and inorganic materials)[1–3] and their numerous potential applications (as lubricants, fuel additives and electrolytes, in separation processes, heat storage, synthesis and catalysis, among others),[4–7] great research efforts have been conducted to their better understanding over the last few decades.

A subset of ILs is that of protic ionic liquids (PILs), first discovered in 1914, when Walden[8] reported the description of ethylammonium nitrate (EAN) and classified it as an IL whose melting point is 287.6 K. These ILs are formed by proton transfer from a Brønsted acid to a Brønsted base.[9–11] The existence of this exchangeable proton is the main difference between PILs and aprotic ionic liquids (AILs) and gives rise to an extended hydrogen bond network, which not only resembles the three-dimensional hydrogen bond network of water,[12,13] but it is also responsible for their special set of properties and their highly ordered structure.[9,11,14]

The amount of articles studying the properties of PILs is not comparable to those on AILs (amongst which it is worth mentioning the firt computational work performed by Canongia-Lopes and Pádua[15] that reported the formation of segregated domains), but relevant contributions have already been reported that shed some light on their peculiar behavior.[14,16–21] For example, Greaves *et al.*[9,11] published several thermal and physicochemical properties of a series of PILs, including glass transition, melting point, boiling point, density, refractive index, viscosity, ionic conductivity, and air-liquid surface tension. In another experimental work, Atkin and Warr investigated the bulk structure of EAN and propylammonium nitrate (PAN) by using small-angle neutron scattering (SANS).[22] They reported the existence of a L_3-sponge-like bulk structure of polar and non-polar domains, these nanoscale heterogeneities being favoured by the solvophobic interactions between alkyl groups, as well as by the electrostatic and hydrogen bonding attractions between the ammonium cation and nitrate anion. This same sponge-like structure in bulk PAN was also reported by Hayes *et al.*[23] using empirical potential structure refinement (EPSR). The resultant amphiphilic PAN nanostructure is more pronounced and with a larger non-polar domain size than that observed in EAN due to the extra methy-

[a] *Grupo de Nanomateriais e Materia Branda, Departamento de Física da Materia Condensada, Universidade de Santiago de Compostela, Campus Vida s/n E-15782, Santiago de Compostela, Spain*
[b] *CEA-Grenoble, 17 Rue des Martyrs, Grenoble 38054, France*
[c] *Facultade de Ciencias, Universidade da Coruña, Campus A Zapateira s/n E-15008, A Coruña, Spain*
[d] *Department of Chemistry, Sapienza University, P. le Aldo Moro 5 Roma, IT 00185, Italy*
* *E-mail: olga.russina@uniroma1.it, luismiguel.varela@usc.es*

lene unit. Besides, Kennedy and Drummond observed the formation of large aggregates of the constituent ions in several PILs by employing electrospray ionization mass spectrometry (ESI-MS).[24] They showed that the $C_8A_7^+$ species (C = cation, A = Anion) was the most abundant and that the formation and size of clusters was dependent on the nature of the anion and cation. This nanostructure is known to occur in imidazolium-based ILs with alkyl chains $> C_4$, whereas chains as short as C_2 are enough to induce nanostructuring of primary ammonium based PILs.[22] Moreover, the spatial dimension of the nanodomains in ILs is known to be controlled by the length of the alkyl chains in their constituents. In a recent article we reported a systematic study of the effect of the cationic chain length and the degree of hydrogen bonding on several equilibrium and transport properties of EAN, PAN and butylammonium nitrate (BAN) by means of several experimental techniques.[25] All our observations reflected the lower hydrogen bonding degree of the PILs with the longer chains, which is due to to enhanced hydrophobic interactions with the cationic chain length of the PILs.

Concerning solutions in PILs, the first contributions on their structure have just been reported by Hayes *et al.*[26] and by some of us[27] using, respectively, neutron (WANS) and X-ray scattering (WAXS), combined with reverse Monte Carlo simulation. In them, salt cations are clearly seen to be dissolved into the polar domains of the IL bulk. Upon this solvation process, IL nanosegregation of the PILs persists, only slightly influenced by the salt addition, and crystalline-like organizations are adopted by the added salt in the polar nanocavities of the amphphilic IL.[27]

Although many physicochemical properties of PILs are now better characterized, it must be said that we are still far from having a complete molecular understanding of dynamical and structural properties of PILs. In this regard, computational simulations are crucial in order to overcome the limitations of experimental research and to get a systematic understanding of the interaction mechanisms between the ions. However, the number of works using computational methods are still very scarce[23,28–32] and, up to our knowledge, only a few publications based on molecular dynamics (MD) simulations have been reported so far.[33–36] In one of the MD studies that have been published to the date, Umebayashi *et al.*[33] analyzed the liquid structure of EAN and found that $[NO_3]^-$ anions significantly interact not only with the ammonium group but also with the alkyl chain of the cations. Their simulations also supported relatively short alkyl chain aggregation as proposed by Atkin and Warr.[22] In addition, Zahn *et al.*[34] performed *ab initio* MD simulations of the PIL monomethylammonium nitrate (MMAN) to investigate its dynamics. Their results exhibited a fast fluctuating hydrogen bond network in which, on average, one hydrogen bond acceptor and one donor site in each ion pair remain free. The structural heterogeneity of EAN, PAN and BAN was also studied by Song *et al.*[35] They found the formation of a distorted NH···O hydrogen bonded network structure regardless of the alkyl chain length, in which nitrate anions usually bond to the charged ammonium headgroup of the cation, and the uncharged alkyl chains aggregate with each other. Finally, this same year we reported the first (up to our knowledge) MD study of the structure of mixtures of a PIL with an inorganic salt, specifically lithium nitrate with EAN,[36] and we found that Li^+ cations placed themselves in the polar domains of the amphiphilically nanostructured PIL, forming solid-like aggregates with the anions in the bulk.

Focusing on the role of ILs as electrolytes for lithium and lithium-ion batteries, most of the studies have been devoted to the analysis of AILs, whereas only Menne *et al.*[37,38] have considered PILs as being a good and cheaper alternative to conventional electrolytes. As it is well-known, obtaining information at the molecular level about the structure and solvation process of these liquids is of fundamental importance for a further understanding of their properties and, thus, improving their performance in this type of applications. In order to provide an insight into the behavior of this kind of ILs we carried out a series of MD simulations of several PILs and their mixtures with alkaline salts.

Continuing with our previous studies,[25,27,36] and trying to further understand the structural features of salt solvation in PILs, in this work we present an experimental and computational room-temperature study of the structure of mixtures of lithium nitrate with three members of the most studied family of PILs, alkylammonium nitrates: EAN,[36] PAN and BAN. To access structural information we performed small angle X-ray scattering (SAXS) to see the influence of the added salt and the alkyl chain length on the nanostructuring of the IL, and computationally examined the evolution of the radial distribution functions, spatial distribution functions, coordination numbers, degrees of hydrogen bonding and cage autocorrelation functions.

After this introduction we include a section describing the computational details of our study, which is followed by a discussion of the obtained results. Finally, we summarize our main conclusions.

2 Experimental and computational details

2.1 Chemical, density and small-angle X-ray scattering measurements

EAN was purchased from IOLITEC with a purity degree of $> 97\%$, and it was used as received. $LiNO_3$ ($> 99.9\%$) was a Merck product, and it was used as received. Density was continuously and automatically measured at 298.15 K using a DSA 5000 Anton Paar density and sound velocity analyzer. This device is equipped with a latest-generation vibrating tube

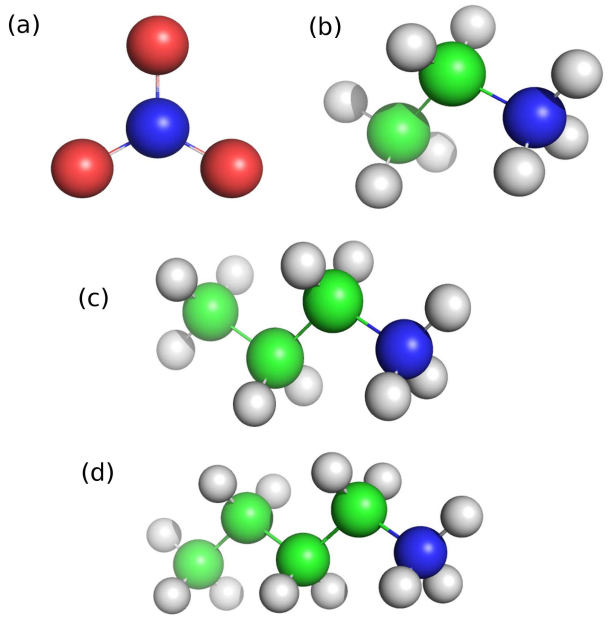

Fig. 1 Molecular structure of (a) nitrate anion, (b) ethylammonium cation, (c) propylammonium cation and (d) butylammonium cation. All of them were modeled using an all-atom representation

for density measurements with a resolution of $\pm 10^{-6}$ g cm^{-3}. Temperature was controlled to within $\pm 10^{-3}$ K by means of a Peltier module. The densimeter was calibrated with dry air and distilled water at known pressure and temperature.

SAXS measurements were conducted at the ID02 beamline at ESRF. The beamline makes use of an instrumental setup that covers the momentum range Q = 1-11 nm^{-1}. Measurements were performed at 298.15 K using a thermostated bath. The samples were kept inside a temperature controlled flow-through cell with an internal diameter of 1.9 mm. The corresponding empty-cell contribution was subtracted.

2.2 Simulation details

MD simulations of pure PAN and BAN, whose schemes are shown in Figure 1, as well as their mixtures with $LiNO_3$ at $T = 298.15$ K and $P = 1$ atm, were carried out using the GROMACS 4.5.4 package.[39] With regard to the parametrization of the ions, the OPLS-AA force field was used, which is an all-atom version of the OPLS force field that models every hydrogen atom bonded to carbon explicitly and whose details have reported in Ref. 40.

Propylammonium and butylammonium cations were built by adding the corresponding number of sites and maintaining the same charge of the alkyl chain as in EAN,[36] and lithium cations were modelled by a single site of charge $+1$ whose Lennard-Jones parameters are $\sigma = 1.25992 \cdot 10^{-1}$ nm and $\varepsilon = 2.615 \cdot 10^{+1}$ kJ/mol. The rest of the details of the simulations have been reported elsewhere.[36]

Due to the fact that our experimental measurements of the density showed that the solubility limits are $\%_{salt} = 18.0$ and $\%_{salt} = 15.4$ for PAN and BAN, respectively, the salt molar percentages simulated in all the systems ($\%_{salt}$={0, 5, 10, 15, 20 and 25}) covered the whole range of concentrations up to saturation and some metastable concentrations above this point. All the initial configurations were built by randomly inserting 300 ionic pairs of IL in a cubic box; with the exception of the percentages $\%_{salt}$= 5 and 10, for which we considered 1000 and 450 ionic pairs with the aim of having enough salt to yield statistically significant trajectories. The number of lithium salt molecules was calculated for each situation by considering each ionic pair as a single unit in the calculation of mole fractions.

For each molar percentage of salt, the system was equilibrated for 20 ns in the isothermal-isobaric (NpT) ensemble applying periodic boundary conditions. We have employed 20 ns long simulations, a time long enough to ensure complete equilibration and sampling of relevant enough regions of the phase space. One must recall to this respect that the experimental bulk density of the IL and its mixtures is reached after 0.5 ns, and the correlation of the ions velocities are completely dumped out after 1 ns. Then, the results of an additional 10 ns–long simulation in the isothermal-isobaric ensemble were used for the analysis of the structure of the mixtures.

3 Results and discussion

SAXS data from binary mixtures of alkylammonium nitrates (PAN and BAN) and $LiNO_3$ at ambient conditions are shown in Figure 2. Data for EAN-$LiNO_3$ mixtures in the same concentration range and conditions have been recently published by some of us.[27]

Neat alkylammonium nitrates have been studied in the past using diffraction techniques. Here we concentrate on those studies referring to small angle X-ray/neutron scattering techniques. In 2008 Atkin *et al.* observed the existence of a low-Q feature in EAN and PAN[22] extending the results[41] of some of us on AILs. Greaves and coworkers extended this investigation to longer members of the series up to pentylammonium nitrates[42] and similar results were obtained by Song and coworkers.[35] These structural features have been rationalised in terms of nanoscale segregated morphology in ILs as a consequence of their inherent amphiphilicity that leads to a polar vs apolar domains segregation. In several ILs the characteristic size associated to this structural feature (that is estimated as given by $D \sim 2\pi/Q$, Q being the position of the low-Q peak) is found to depend linearly on the number of CH_2/CH_3 groups in the side alkyl tail and this is also the case for alkyl

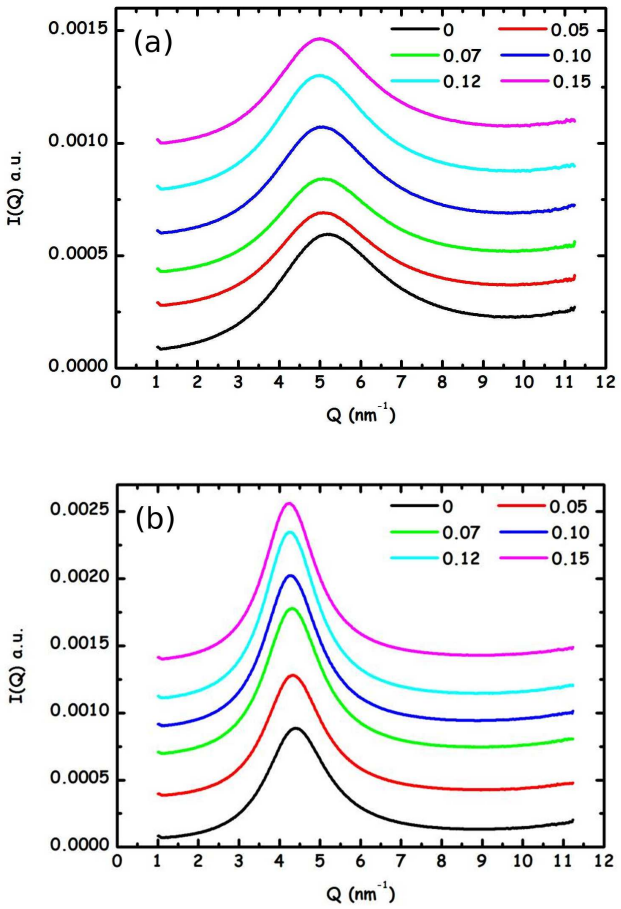

Fig. 2 Small angle X-ray scattering data from binary mixtures of (a) propylammonium and (b) butylammonium nitrate-$LiNO_3$ at ambient conditions. The legend refers to lithium salt content expressed in molar fraction. Data have been vertically shifted for clarity purposes

ammonium nitrates. SAXS data from EAN-$LiNO_3$ mixtures have been recently reported by us [27] together with a modelling of wide angle X-ray scattering data, while wide angle neutron scattering data from different isotopically substituted mixtures were investigated by Atkin *et al.* [26]

The existence of low-Q peaks associated to structural features in the mixtures was also confirmed by means of MD simulations, as shown in Figure 3, where MD SAXS calculations for a mixture of BAN with a 10% of lithium salt are compared to the experimental observations. As can be observed in the inset, the agreement for this concentration is very good, and this is also the case for most of the studied concentration, as shown in the inset.

In Figure 4, we show the $LiNO_3$ concentration dependence of the characteristic scales in the three sets of mixtures. Together with the data obtained for PAN and BAN, we also report data from Ref. 27. We notice that the three sets of solutions show an approximately linear trend for D vs $[Li]^+$ content. These data sets show that the characteristic spatial scales for the mesoscopic order in these mixtures fall in the range from 9 to 16 Å, with progressive increase of this size with increasing $[Li]^+$ content.

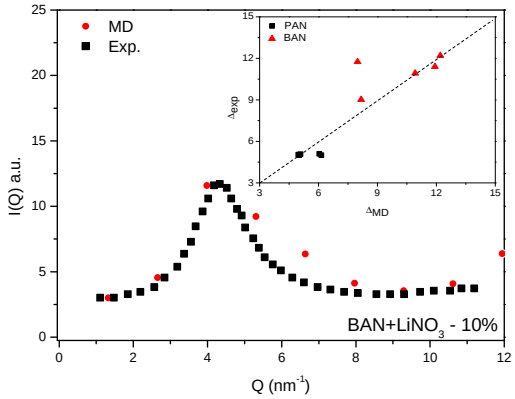

Fig. 3 Small angle X-ray scattering data from MD simulations of BAN mixed with a 10% of $LiNO_3$. The inset shows the experimental heights of the low-Q peaks vs the corresponding MD predictions for the various studied concentrations of mixtures with PAN and BAN. The dashed line corresponds to perfect agreement.

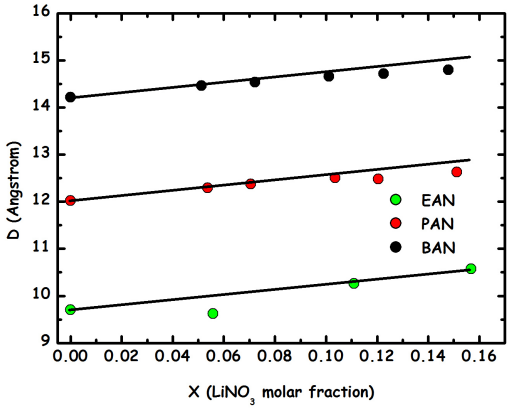

Fig. 4 Characteristic spatial sizes (D) extracted from small angle X-ray scattering data from binary mixtures of ethyl-, propyl- and butyl-ammonium nitrate/$LiNO_3$ (EAN, PAN and BAN, respectively) at ambient conditions. The three lines are parallel and have been obtained by a linear fitting to the EAN-$LiNO_3$ trend excluding the 0.055 mf value.

It is noteworthy that at intermediate concentrations EAN-$LiNO_3$ mixtures show deviations from such a linear trend and

D at 0.06 molar fraction (mf) in lithium salt is smaller than the value for neat EAN. At higher $[Li]^+$ content, however, D tends to grow and gets larger than in neat EAN. This kind of behaviour explains the observation done in a recent paper by Atkin *et al.*, where they report experimental neutron scattering data for the case of 0.10 molar fraction in $[Li]^+$ salt and they notice that for that concentration the low-Q peak position falls at larger Q values than for neat EAN. Our present X-ray data set somehow confirms that a concentration regime exists where the peak position shifts towards larger Q values (decrease in D values), but this is followed by a concentration range where the peak shifts towards smaller Q values (increase in D values). It is also noteworthy that the same trend is not observed for the case of PAN and BAN mixtures with lithium salt, as the peak position (characteristic spatial scale) progressively shifts downwards (upwards) upon lithium salt addition. Moreover, we notice that, even when the 0.055 mf data deviates ca. 2%, the characteristic spatial sizes in the EAN-$LiNO_3$ mixtures follow a linear trend with a slope $dD/dx_{[Li]^+}$ = 5 Å/mf. This trend is also followed by PAN and BAN mixtures with $LiNO_3$, in the dilute regime below $x_{[Li]^+} = 0.1$. This observation might imply subtle structural effects played by the lithium addition on the sponge-like morphology in bulk alkylammonium nitrates.

Hence, our X-ray data suggest that the characteristic size of the mesoscopic correlations increases with salt addition. In order to get further understanding of this phenomenon, we performed MD simulations of the studied mixtures. As density is one of the properties most easily comparable with experimental data, it is worth making a comparison between computational and experimental density results to estimate the validity of the force field employed in our MD simulations and its accuracy to represent the behavior of a given system. Figure 5 shows the salt concentration dependence of both experimental and simulated density for mixtures of EAN (which had been previously reported in Ref. 36), PAN and BAN with $LiNO_3$. It can be seen there that the predicted densities of the systems involving PAN and BAN are in excellent agreement with the experimental values. In view of these results we can be reasonably confident about the ability of our force field to reproduce the structural properties and the solvation process of these PILs. However, it must be taken into account that, since the force field employed is non-polarizable, we cannot get quantitatively accurate predictions for the dynamic properties of lithium ions (as we proved in Ref. 43). It can be also seen that all the mixtures show the same linear increase with salt concentration previously reported for lithium salts in AILs and in EAN.[36,43] In addition, the slope of the density is practically independent of the IL cation alkyl chain length. These features suggest that added salt ions are solvated into the polar nanoregions of the mixture, whose density increases upon salt addition either by breaking hydrogen bonds in these regions

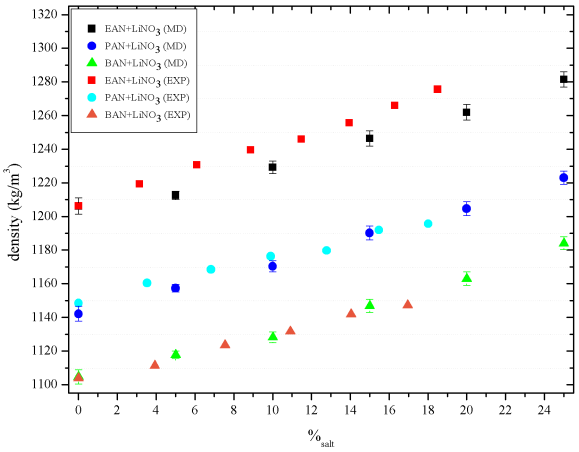

Fig. 5 Simulated and experimental densities at $T = 298.15$ K of EAN (squares), PAN (dots) and BAN (triangles) mixed with lithium salts with a common anion as a function of the lithium salt concentration. Data for EAN were taken from Ref. 36.

and/or by forming clusters with the $[NO_3]^-$. Moreover, if we recall that the partial molar volume of a solute of molar mass M_2, $\bar{V}_2$, in an IL of density ρ_0 can be approximated for constant partial molar volume (i.e. when the partial molar volume and the apparent molar volume are equal) as

$$\bar{V}_2 \simeq \frac{1}{\rho_0}\left(M_2 - \frac{\partial \rho}{\partial c}\right) \quad (1)$$

where c is the molar concentration of the salt, we can easily conclude that, as the chain length of the cation IL increases, the partial (equiv. apparent) molar volume of the salt increases, which can be seen as an indicative of an enhanced influence of the addition of salt on the thermodynamics properties of the systems the longer the IL cation alkyl chain length.

These features can be also observed in Fig. 6, in which we analyze the concentration dependence of the well-known hydrogen bond network between nitrate anions and alkylammonium cations. For this purpose, we calculated the evolution of the average number of hydrogen bonds per molecule by normalizing the number of H-bonds by the number of ions (excluding lithium cations), as explained in Ref. 36. In addition, since the large organic parts of the molecules of these systems are not involved in hydrogen bonds, the fraction of hydrogen-bonded atoms is more informative about the relative extent of hydrogen bonding. Accordingly, we included the analysis of the average number of hydrogen bonds per atom in the ionic pair in order to clarify the effect that the cationic chain length has on this property. The criteria considered in GROMACS for determining the presence of a hydrogen bond are purely geometrical; that is to say, the distance between acceptor and hydrogen must be lower than or equal to 0.35 nm, and

the angle between acceptor-donor-hydrogen must be smaller than or equal to 30°. In this case, the three-dimensional network results from the hydrogen bond taking place between the oxygen atoms of all the nitrates that are present in the mixture (regarded as acceptors) and the hydrogen atoms of the ammonium headgroup of the cation (considered as donors). In Fig. 6.a we can observe a linear decrease in the average number of hydrogen bonds regardless of the alkylammonium cation chain length as the lithium salt concentration increases, which shows a gradual break up of the IL H-bond network due to the $[Li]^+$ cations placing themselves in the polar domains of the network. This is the same tendency previously reported for solutions of EAN with $LiNO_3$.[36] Furthermore, Fig. 6.b evidences that the hydrogen bonding extent of the PILs is lower the longer the cation chain length, since the formation of a hydrogen bond is more difficult due to the higher size of the apolar domains and the greater distance between ions.[25] Interestingly, we can see in Fig. 6.a that the number of hydrogen bonds per molecule is practically the same for the various studied PILs, and, even more interestingly, the rate of change of this number with concentration is practically identical for the different ILs. This further reinforces the notion that changes on the hydrogen bond network with added salt are confined to the polar nanoregions of the mixture, where $[Li]^+$ electrostrictive ionic field forces reorientation of $[NO_3]^-$ anions, removing them from H-bonds with the $[XA]^+$ cations. However, when we come to analyze the number of hydrogen bonds per atom, we see that the average number of H-bonds per atom in the ionic pair decreases slightly faster for mixtures of PILs with shorter alkyl chains, since longer cations have more atoms that do not participate in a hydrogen bond. Nevertheless, it must be pointed out that, since mixtures of PILs with longer alkyl chains are hydrogen bonded to a lesser extent, H-bonds breakage is expected to have a deeper impact on the properties of the mixture the longer the alkyl chain length of the solvent cation.

A strong segregation of polar and apolar domains in the mixtures can be clearly observed in Fig. 7, in which we show several snapshots of the simulation box of a 25% of $LiNO_3$ mixed with PAN and BAN. As we previously found in solutions of $LiNO_3$ in EAN,[36] the vast majority of the $[Li]^+$ cations are located in the polar regions of the bulk, decreasing the interaction strength between nitrate anions and ammonium groups and gradually breaking the strong hydrogen bond network existing in bulk PILs. Moreover, these snapshots support the picture of larger apolar domains as the IL cation alkyl chain length increases, in agreement with the study of Hayes *et al.*[21]

Further evidence of lithium cations solvation in the bulk system and its influence on the IL network can be obtained by quantifying spatial structure through the analysis of the radial distribution function (RDF),

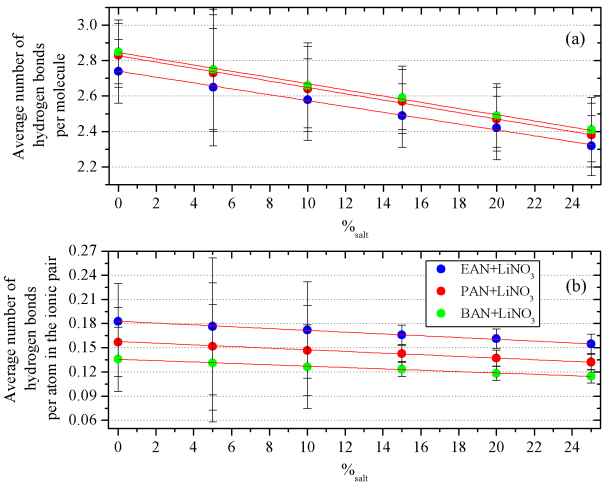

Fig. 6 (a) Concentration dependence of the average number of hydrogen bonds per molecule for mixtures of $LiNO_3$ with EAN (blue), PAN (red) and BAN (green). (b) Concentration dependence of the average number of hydrogen bonds per atom in the ionic pair for solution of $LiNO_3$ in EAN (blue), PAN (red) and BAN (green). The lines are guides for the eye. Data for EAN were taken from Ref. 36.

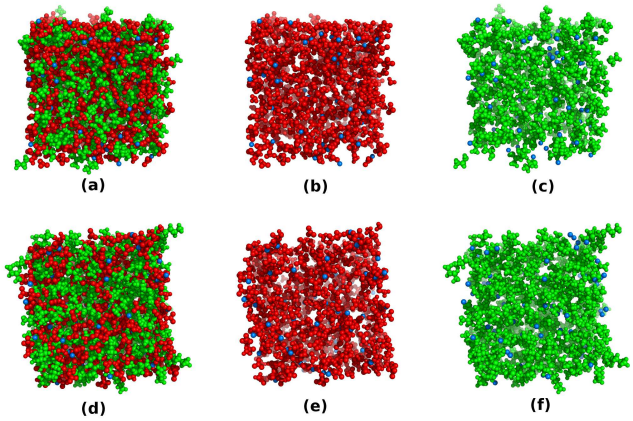

Fig. 7 Snapshots of the simulation box of the mixtures of 25% of $LiNO_3$ with PAN (a, b, c) and BAN (d, e, f) at 298 K. The representations of the bulk structure include: (a) and (d) the whole system, (b) and (e) nitrate anions, ammonium group of the IL cation (polar domain - red) and lithiums (blue), (c) and (f) chain of the IL cation (apolar domain - green) and lithiums (blue). The relative size of lithium has been exaggerated for clarity.

$$g_{ij}(r_{12}) = \frac{1}{\rho_i \rho_j} \sum_{i,j}^{N} \langle \delta(\vec{r}_1 - \vec{r}_i) \delta(\vec{r}_2 - \vec{r}_j) \rangle \qquad (2)$$

where ρ is the number density, N stands for the number of particles in the system, i and j run over all the species, and brackets indicate the ensemble average. It must be clarified that for the calculations of the RDFs involving the alkylammonium cation we only took into account the four atoms in the ammonium or methyl groups, and that all RDFs presented in this paper were calculated by considering the center of mass of the defined groups, except in the case of hydrogen-oxygen $g(r)$'s (of ammonium group and nitrate, respectively), for which an average of the atomic RDFs was calculated.

The lithium salt concentration dependences of the RDFs involving the ions of the PILs are presented in Figs. 8 and 9 for mixtures with PAN and BAN, respectively. In particular, these two figures show $g(r)$'s between (a) $[NO_3]^-$ anion-ammonium group of the IL cation, (b) $[NO_3]^-$ anion-methyl group of the IL cation, and (c) hydrogen-oxygen (of ammonium group of the IL cation and nitrate anion, respectively). In a similar way to that reported for EAN,[36] the strongest coordination is found between $[NO_3]^-$ and $[NH_3]^+$. The strength of this interaction decreases in a more pronounced way than that between $[NO_3]^-$ and IL cation alkyl groups with the addition of lithium salt to the system, which once again indicates that lithium cations are accommodated into the polar domains of the bulk inducing a rupture of the H-bonds between IL ions in the nanoregion. Moreover, the position of the first peaks of the $g(r)$'s of the IL components does not vary as the concentration of lithium salt increases, which indicates that the structure of these liquids is not significantly changed by salt addition, but for its hydrogen bond extent in the polar nanoregions. However, increasing the length of the cation alkyl chain does have an impact on the amphiphilic nanostructure of the bulk. Firstly, the height of the first peak in the RDF between nitrate anion and ammonium group (Fig. 8.a, Fig. 9.a in this paper, and Fig. 2.a in Ref. 36) clearly increases upon increasing the cation alkyl chain, which is indicative of an increasing segregation of the fluid, giving rise to better defined polar domains of the PILs with alkyl chain length.[21] Additionally, the decrease of the height of the first peak in the $g(r)$ between nitrate anion and methyl group (Fig. 8.b, Fig. 9.b in this paper, and Fig. 2.b in Ref. 36) reveals a reduction in the coordination between these two groups of atoms, which is due to the existence of larger and better defined apolar domains and leads to a looser nanostructuration more similar to a sponge in the mixtures with longer alkyl chains. Finally, there are no substantial differences in the distance between the atoms that participate in the hydrogen bond (Fig. 8.c, Fig. 9.c and Fig. 2.c in Ref. 36), and we obtained an average $O\cdots H$ distance of 0.18 nm, in agreement with the conclusions drew by Bodo *et al.*[29] However, the number of atoms at that distance decreases with the addition of salt, as reflected in the height of the peak of 9.c.

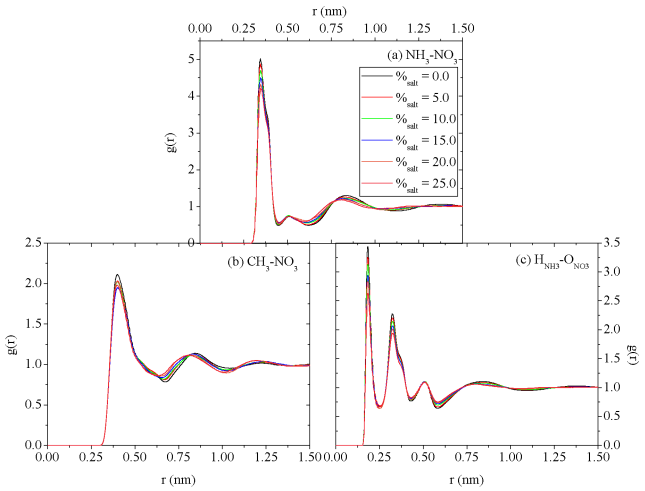

Fig. 8 RDFs of (a) nitrate anion-ammonium group, (b) nitrate anion-methyl group and, (c) hydrogen-oxygen (of ammonium group and nitrate anion) as a function of the lithium salt concentration in solutions of $LiNO_3$ in PAN at 298.15 K.

Figures 10 and 11, which show the RDFs involving $[Li]^+$ cations and both ionic species of the PILs, provide us with further evidence of the location of lithiums in the bulk mixtures. The greater height of the peaks of the RDFs between $[NO_3]^-$ anions and $[Li]^+$ and their positions at shorter distances show that lithiums are mainly coordinated with nitrate anions, as we found in mixtures with EAN.[36] It is also noteworthy that the interaction of lithium cations with both nitrate anions and the ammonium group of the IL cations increases as the degree of hydrogen bonding decreases (that is, as the alkyl chain length of the IL cation increases), which is compatible with lithium being constrained to lie in progressively more compact, denser polar nanoregions. In the case of PAN and BAN, the first solvation shell of lithiums around nitrates is composed of a double peak (Figs. 10.a and 11.a) as in the case of EAN mixtures, which indicates that $[Li]^+$ cations can be found in two different conformations: bidendate (corresponding to the first peak) and monodendate (corresponding to the second peak). Although the monodendate conformation is the more abundant independently of the alkyl chain length of the IL cation, it seems that the relative abundance of this way of coordination becomes comparable to that of the bidendate one when increasing the length of the IL cation alkyl chain, since the heights of the peaks tend to be more similar. This is indicative of a compaction of the polar regions as the alkyl chain length of the IL cation is increased, associated to a decrease in their volume fraction decrease via a "dilution effect".

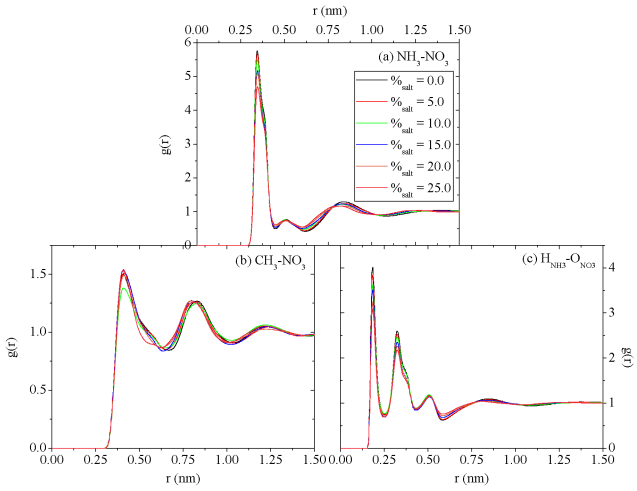

Fig. 9 RDFs of (a) nitrate anion-ammonium group, (b) nitrate anion-methyl group and, (c) hydrogen-oxygen (of ammonium group and nitrate anion) as a function of the lithium salt concentration in solutions of $LiNO_3$ in BAN at 298.15 K.

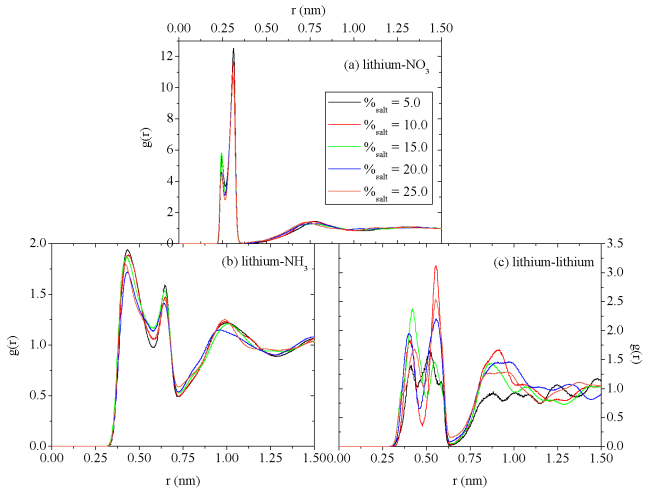

Fig. 10 RDFs of (a) lithium-nitrate anion, (b) lithium-ammonium group and, (c) lithium-lithium as a function of the lithium salt concentration in solutions of $LiNO_3$ in PAN at 298.15 K.

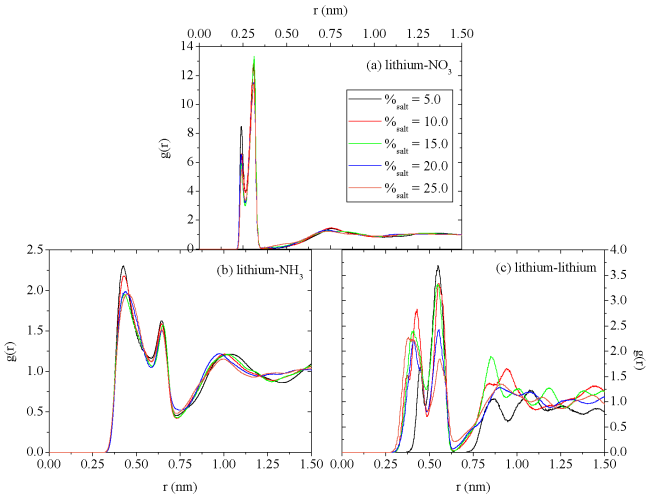

Fig. 11 RDFs of (a) lithium-nitrate anion, (b) lithium-ammonium group and, (c) lithium-lithium as a function of the lithium salt concentration in solutions of $LiNO_3$ in BAN at 298.15 K.

Another interesting tool for shedding light on the bulk structure is the spatial distribution function (SDF), which provides useful information about the three-dimensional density distribution of atoms around a central molecule. In this case, the SDFs were determined by fixing a distance from the central molecule, which corresponds to the position of the first (and also second for calculations involving lithiums) maximum of the RDFs, and calculating the angular probability distribution of finding an atom at a specific point in the mixture. All the reported SDFs correspond to the different species around the nitrate anions, which are indeed plane molecules. The reference plane corresponds to the plane of the molecule itself, and all the nitrate anions have been rotated so that their planes are identically oriented before calculating the corresponding average angular probabilities. Thus, Fig. 12 shows the heat maps of the angular distribution of (a), (b), (e) and (f) lithium cations, (c) and (g) nitrogen in the $[NH_3]^+$ group of the IL cation and (d) and (h) nitrogen in the $[NO_3]^-$ anion at an specific distance from a central nitrate for the mixtures of a 15% of $LiNO_3$ with PAN (a, b, c, d) and BAN (e, f, g, h). The main observed effect of increasing the alkyl chain length of the IL cation is that, despite the better defined polar and apolar domains the longer the alkyl chains, the polar domains of PAN and BAN mixtures seem to be, on average, less ordered than those in EAN mixtures.[36] This is reflected in the much more diffuse heat maps of the distributions of lithium cations (a, b, e, f) around the nitrates, where we see that $[Li]^+$ are neither forced to be located in the bisectrix of the angle formed by two oxygens and the central nitrogen of the anions (bidendate conformation) nor facing the nitrate oxygens (monodendate conformation). Hence, these two conformations around a

central $[NO_3]^-$ are less clearly observed than in mixtures with EAN.[36] A similar effect, although slightly less marked in the case of the nitrogen of the ammonium cation, is observed for both alkylammonium cations and nitrate anions surrounding a central $[NO_3]^-$. This increment of the orientational disorder in the nanoregions could be associated to the collapse of the directional hydrogen bond network inside the polar nanoregions.

The lithium salt concentration dependence of the coordination numbers of the ions in the mixtures is also an informative variable. The results of numerically integrating the function $4\pi r^2 \rho g(r)$ (where ρ is the numerical density of the molecules around an specific central ion, lithium in this case, and $g(r)$ is one of the RDFs plotted in Figs. 8.a, 9.a, 10 and 11) up to the end of the first solvation shell (given by the first minimum of the corresponding RDFs) are shown in Fig. 13. In general, there are no significant diferences between the coordination numbers in solutions of $LiNO_3$ in EAN, PAN and BAN, except for the fact that the number of alkylammonium cations solvating a given lithium slightly decreases with increasing the alkyl chain length, going from 3 in EAN to less than 2.5 in BAN. The reason why this change takes place is the increase of the thickness of the apolar domains with increasing IL alkyl chain length, as indicated by bulk liquid correlation length (determined from low Q Bragg peaks). Additionally, a slight decreasing of the coordination numbers of alkylammonium cations around a central $[Li]^+$ can be observed upon salt addition. This could be explained by an increase of the polar domains, since this kind of expansion would lead to fewer cations in a solvation shell with the same size. The swelling of the polar domains is due to the increase in the number of ions in these regions associated to a decrease of the number of H-bonds. However, the observed increase in density would be associated to an increase in the ion densities in the polar regions, confirmed not only by an increase of $[NO_3]^-$ densities in the polar regions from 1.25 $[NO_3]^-/nm^3$ for pure PIL to 1.71 $[NO_3]^-/nm^3$ from a mixture with a 20% of lithium salt, but also by a decreasing of the position of the first peak in the anion-anion RDFs as the amount of salt increases. We can also deduce an expansion of the apolar domains with the addition of lithium salt, which is suggested by a slight decrease of $[CH_3]$ densities in the apolar regions. On the other hand, in mixtures with PAN and BAN a central $[Li]^+$ is also surrounded by almost four $[NO_3]^-$ in its first coordination layer and an average of nearly one lithium in its second solvation shell over the whole miscibility range, as we reported for EAN.[36] This is in agreement with neutron diffraction[23,42,44] and SAXS[27] experiments, which have shown that the underlying bulk nanostructure does not significantly undergo changes (and ion-ion correlations) as IL alkyl chain length is increased.

In order to analyze the behaviour of lithium cations within their first coordination shell, we calculated the velocity auto-

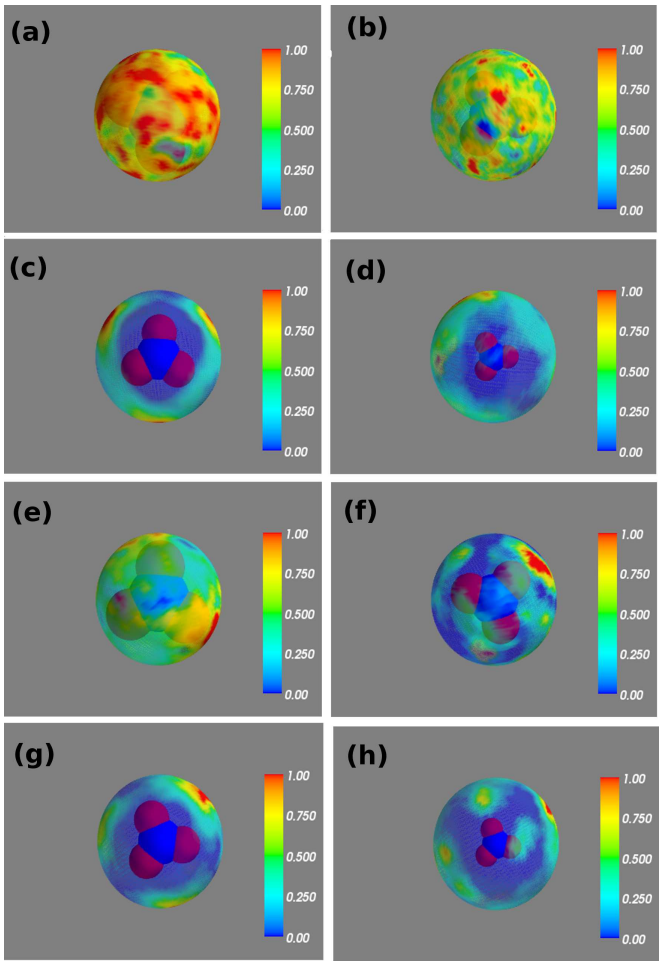

Fig. 12 SDF plots of lithium first (a), (b), and second peaks, (e) and (f), nitrogen in the ammonium group of the alkylammonium cation (c) and (g), and nitrogen in the nitrate anion (d) and (h) as a function of the angular position around a central nitrate anion in mixtures of a 15% of $LiNO_3$ with PAN (a, b, c, d) and BAN (e, f, g, h). The distance at which SDFs were calculated corresponds to the first (or second in the case of lithiums) maximum of the RDFs: (a) and (e) first peak (0.24 nm) in Figs. 10.a and 11.a, respectively; (b) and (f) second peak (0.31 nm) in Figs. 10.b and 11.b, respectively; (c) and (g) first peak (0.34 nm) in Figs. 8.a and 9.a, respectively; (d) and (h) first peak (0.50 nm) in anion-anion RDFs.

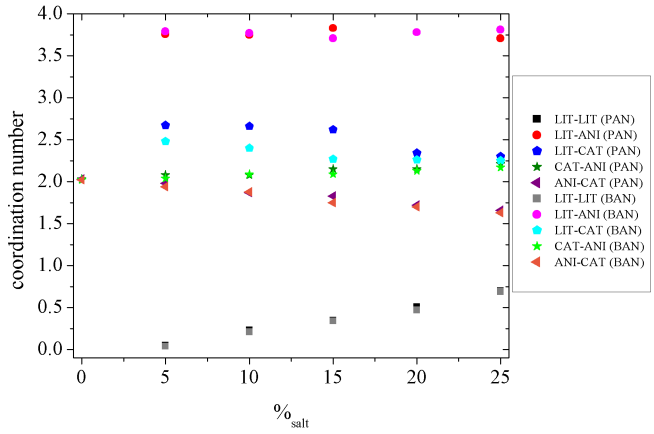

Fig. 13 Concentration dependence of the coordination numbers of lithium cations (black squares-PAN, grey squares-BAN), nitrate anions (red circles-PAN, pink circles-BAN), and alkylammonium cations (dark blue pentagons-PAN, light blue pentagons-BAN) surrounding a central lithium cation in mixtures of PAN and BAN with $LiNO_3$. The number of nitrate anions around a central alkylammonium cation (dark green stars-PAN, light green stars-BAN) and vice versa (violet triangles-PAN, orange triangles-BAN) are also included.

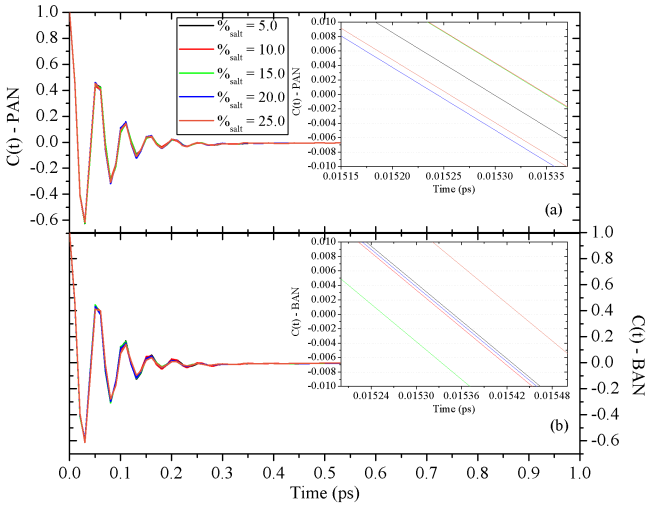

Fig. 14 Evolution of the lithium cations VACFs with the amount of lithium salt in mixtures with (a) PAN and (b) BAN. The insets show the concentration dependence of the collision time.

correlation functions (VACFs) of these ions, which are shown in Fig. 14. The normalized VACFs are determined as

$$C(t) = \frac{\langle \vec{v}(t) \cdot \vec{v}(0) \rangle}{\langle \vec{v}(0) \cdot \vec{v}(0) \rangle}, \quad (3)$$

where $\vec{v}(t)$ is the velocity of the center of mass of the molecule at time t and the brackets indicate the ensemble average. We have performed high-frequency calculations (time step = 1 fs) and further verified that the results are not modified if we increase the saving frequency to 2 fs. The first thing we observe in the two panels of these figures is that the VACFs are almost identical for PAN and BAN mixtures, once again reflecting the relative independence of the solvation environment of lithium on the alkyl chain length of the IL cation, which can only be explained if the salt cation goes into the polar nanodomains of the mixture. Moreover, in exactly the same way as it was found in mixtures with EAN,[36] this magnitude shows a clear oscillatory behavior that reveals that lithium cations experience a rattling motion inside the "cages" formed by they nearest neighbors, that is, the four nitrate anions that form their first coordination shell. Additionally, these oscillations are in all cases completely damped out after 0.3 ps. However, in mixtures of $LiNO_3$ with PAN and BAN we could not find a clear tendency of the collision times (indicated by the first zero of the VACF) with the amount of salt, but this is probably due to the uncertainties related to the low number of frames in the trajectories for these short times.

4 Conclusions

In the present paper, SAXS and MD simulations have been used with the aim of elucidating the bulk structure and the solvation process in mixtures of PAN and BAN with $LiNO_3$ at room temperature. For this purpose, we analyzed the influence of the amount of salt and of the alkyl chain length of the IL cation on several properties such as density, radial distribution function, coordination numbers, spatial distribution function, hydrogen bonds and velocity autocorrelation function.

Like we previously showed for mixtures with EAN in Ref. 36, the bulk of PAN and BAN is also nanostructured due to the electrostatic, van der Waals, hydrogen bonding and solvophobic interactions. As a result, charged groups (nitrate anions and cation head groups) interact to form polar domains, whereas alkyl groups tend to associate into apolar domains. This nanosegregation of PILs has a deep impact on the solvation of lithium salts, since their ions are forced to heterogeneously accommodate into the polar network of the IL, coordinating mainly with the nitrate anions and giving rise to crystalline-like structures. On their turn, lithium ions in the polar nanodomains progressively erode the hydrogen bond network of the PIL, decreasing the extent of hydrogen bond of the mixtures and inducing orientational disorder in their polar nanodomains. This effect is more pronounced for PILs whose cations have longer alkyl chains due to the lower degree of hydrogen bonding among their constituents.

Acknowledgement

The authors wish to thank the financial support of Xunta de Galicia through the research projects of references 10-PXI-103-294 PR, 10-PXIB-206-294 PR and GPC2013-043. Moreover, this work was funded by the Spanish Ministry of Science and Innovation (Grant No. FIS2012-33126). All these research projects are partially supported by FEDER. T. Méndez-Morales thanks the Spanish ministry of Education for her FPU grant. O.R. acknowledges the European Synchrotron Radiation Facility for provision of synchrotron radiation facilities and would like to thank Dr. T. Narayanan his kind and competent assistance in exploiting beamline ID02. O.R. acknowledges support from FIRB-Futuro in Ricerca (RBFR086BOQ) and PRIN (2009WHPHRH). Facilities provided by the Galician Supercomputing Centre (CESGA) are also acknowledged.

References

1 P. Wasserscheid and T. Welton, *Ionic liquids in synthesis*, Wiley Online Library, 2003.
2 H. Ohno, *Electrochemical aspects of Ionic Liquids*, John Wiley & Sons, Inc., 2005.
3 S. Zhang, N. Sun, X. He, X. Lu and X. Zhang, *J. Phys. Chem. Ref. Data*, 2006, **35**, 1475–1517.
4 N. V. Plechkova and K. R. Seddon, *Chem. Soc. Rev.*, 2008, **37**, 123–150.
5 D. R. MacFarlane, M. Forsyth, P. C. Howlett, J. M. Pringle, J. Sun, G. Annat, W. Neil and E. Izdorodina, *Acc. Chem. Res.*, 2007, **40**, 1165–1173.
6 Z. Zeng, B. S. Phillips, J.-C. Xiao and J. M. Shreeve, *Chem. Matter.*, 2008, **20**, 12719–2726.
7 J. S. Wilkes, *J. Mol. Catal. A: Chem.*, 2004, **214**, 11–17.
8 P. Walden, *Bull. Russian Acad. Sci.*, 1914, **1800**, 405–422.
9 T. L. Greaves and C. J. Drummond, *Chem. Rev.*, 2008, **108**, 206–237.
10 W. X. M. Yoshizawa and C. A. Angell, *J. Am. Chem. Soc.*, 2003, **125**, 15411–15419.
11 T. L. Greaves, A. Weerawardena, C. F. andgre I. Krodkiewska and C. J. Drummond, *J. Phys. Chem. B*, 2006, **110**, 22479–22487.
12 A. W. K. Fumino and R. Ludwig, *Angew. Chem. Int. Ed.*, 2009, **48**, 3184–3186.
13 W. Xu and C. A. Angell, *Science*, 2003, **302**, 422–425.
14 T. L. Greaves, A. Weerawardena, I. Krodkiewska and C. J. Drummond, *Chem. Rev.*, 2008, **112**, 896–905.
15 J. N. Canongia-Lopes and A. A. H. Pádua, *J. Phys. Chem. B*, 2006, **110**, 3330–3335.
16 X. C. X. Wang, Q. Li and Z. Li, *Langmuir*, 2012, **28**, 16547–16554.
17 V. H. Alvarez, N. Dosil, R. Gonzalez-Cabaleiro, S. Mattedi, M. Martin-Pastor, M. Iglesias and J. M. Navaza, *J. Chem. Eng. Data*, 2010, **55**, 625–632.
18 P. Niga, D. Wakeham, A. Nelson, G. G. Warr, M. Rutland and R. Atkin, *Langmuir*, 2010, **26**, 8282–8288.
19 J. Hunger, T. Sonnleitner, L. Liu, R. Buchner, M. Bonn and H. J. Bakker, *J. Phys. Chem*, 2012, **3**, 3034–3038.
20 C. Zhao, G. Burrell, A. A. J. Torriero, F. Separovic, N. F. Dunlop, D. R. MacFarlane and A. M. Bond, *J. Phys. Chem. B*, 2008, **112**, 6923–6936.
21 R. Hayes, S. Imberti, G. G. Warr and R. Atkin, *J. Phys. Chem. C*, 2014, **118**, 13998–14008.
22 R. Atkin and G. G. Warr, *J. Phys. Chem. B*, 2008, **112**, 4164–4166.
23 R. Hayes, S. Imberti, G. G. Warr and R. Atkin, *Phys. Chem. Chem. Phys.*, 2011, **13**, 13544–13551.
24 D. F. Kennedy and C. J. Drummond, *J. Phys. Chem. B*, 2009, **113**, 5690–5693.
25 S. B. Capelo, T. Méndez-Morales, J. Carrete, E. L. Lago, J. Vila, O. C. J. R. Rodríguez, M. Turmine and L. M. Varela, *J. Phys. Chem. B*, 2012, **116**, 11302–11312.
26 R. Hayes, S. A. Bernard, S. Imberti, G. G. Warr and R. Atkin, *J. Phys. Chem. C*, http://dx.doi.org/10.1021/jp506192d.
27 O. Russina, R. Caminiti, T. Méndez-Morales, J. Carrete, O. Cabeza, L. Gallego, L. Varela and A. Triolo, *J. Mol. Liq.*, 2014, http://dx.doi.org/10.1016/j.molliq.2014.08.007.
28 E. Bodo, P. Postorino, S. Mangialardo, G. Piacente, F. Ramondo, F. Bosi, P. Ballirano and R. Caminiti, *J. Phys. Chem. B*, 2011, **115**, 13149–13161.
29 E. Bodo, S. Mangialardo, F. Ramondo, F. Ceccacci and P. Postorino, *J. Phys. Chem. B*, 2012, **116**, 13878–13888.
30 H. Markusson, J.-P. Belieres, P. Johansson, C. A. Angell and P. Jacobsson, *J. Phys. Chem. A*, 2007, **111**, 8717–8723.
31 R. Hayes, S. Imberti, G. G. Warr and R. Atkin, *Angew. Chem., Int. Ed.*, 2012, **51**, 7468–7471.
32 R. Hayes, S. Imberti, G. G. Warr and R. Atkin, *Angew. Chem., Int. Ed.*, 2013, **52**, 4623–4627.
33 Y. Umebayashi, W.-L. Chung, T. Mitsugi, S. Fukuda, M. Takeuchi, K. Fujii, T. Takamuku, R. Kanzaki and S. Ishiguro, *J. Comput. Chem. Jpn.*, 2008, **7**, 125–134.
34 S. Zahn, J. Thar and B. Kirchner, *J. Chem. Phys.*, 2010, **132**, 124506(1)–124506(13).
35 X. Song, H. Hamano, B. Minofar, R. Kanzaki, K. Fujii, Y. Kameda, S. Kohara, M. Watanabe, S. Ishiguro and Y. Umebayashi, *J. Phys. Chem. B*, 2012, **116**, 2801–2813.
36 T. Méndez-Morales, J. Carrete, O. Cabeza, O. Russina, A. Triolo, L. J. Gallego and L. M. Varela, *J. Phys. Chem. B*, 2014, **118**, 761–770.
37 S. Menne, J. Pires, M. Anouti and A. Balducci, *Electrochem. Commun.*, 2013, **31**, 39–41.
38 S. Menne, T. Vogl and A. Balducci, *Phys. Chem. Chem. Phys.*, 2014, **16**, 5485–5489.
39 D. V. D. Spoel, E. Lindahl, B. Hess, A. R. V. Buuren, E. Apol, P. J. Meulenhoff, D. P. Tieleman, A. L. T. M. Sijbers, K. A. Feenstra, R. V. Drunen and H. J. C. Berendsen, *Gromacs User Manual version 4.0*, http://www.Gromacs.org, 2005.
40 W. L. Jorgensen, *J. Phys. Chem.*, 1986, **90**, 1276–1284.
41 A. Triolo, O. Russina, H.-J. Bleif and E. Di Cola, *J. Phys. Chem. B*, 2007, **111**, 4641–4644.
42 T. L. Greaves, D. F. Kennedy, S. T. Mudie and C. J. Drummond, *J. Phys. Chem. B*, 2010, **114**, 10022–10031.
43 T. Méndez-Morales, J. Carrete, S. Bouzón-Capelo, M. Pérez-Rodríguez, O. Cabeza, L. J. Gallego and L. M. Varela, *J. Phys. Chem. B*, 2013, **117**, 3207–3220.
44 R. Hayes, S. Imberti, G. G. Warr and R. Atkin, *Phys. Chem. Chem. Phys.*, 2011, **13**, 3237–3247.